PERGAMON

International Journal of Plasticity 20 (2004) 403–425

INTERNATIONAL JOURNAL OF Plasticity

www.elsevier.com/locate/ijplas

Effect of solutes on dislocation motion —a phase-field simulation

S.Y. Hu[a,*], Y.L. Li[a], Y.X. Zheng[b], L.Q. Chen[a]

[a] *Department of Materials Science and Engineering, The Pennsylvania State University, University Park, PA 16802, USA*

[b] *Department of Mathematics The Pennsylvania State University, University Park, PA 16802, USA*

Received in final revised form 23 March 2003

Abstract

Based on recent advances in phase-field models for integrating phase and defect microstructures as well as dislocation dynamics, the interactions between diffusional solutes and moving dislocations under applied stresses are studied in three dimensions. A new functional form for describing the eigenstrains of dislocations is proposed, eliminating the dependence of the magnitude of the dislocation Burgers vector on the applied stress and providing correct stress fields of dislocations. A relationship between the velocity of the dislocation and the applied stress is obtained by theoretical analysis and numerical simulations. The operation of Frank–Read sources in the presence of diffusional solutes, the effect of chemical interactions in solid solution on the equilibrium distribution of Cottrell atmosphere, and the drag effect of Cottrell atmosphere on dislocation motion are examined. The results demonstrate that the phase-field model correctly describes the long-range elastic interactions and short-range chemical interactions that control dislocation motion.

Keywords: Solute segregation; Lattice mismatch; Dynamic drag effect; Dislocation dynamics; Phase-field approach

1. Introduction

Solid solution hardening is one of the commonly used mechanisms to strengthen essentially all classes of alloy systems. Solid solution hardening arises from various

* Corresponding author.

0749-6419/$ - see front matter © 2003 Published by Elsevier Ltd.
doi:10.1016/S0749-6419(03)00094-9

interactions between dislocations and solutes such as elastic interactions, electric interactions and chemical interactions (Cottrell et al., 1948; Haasen, 1964; Fridel, 1963; Hirth and Lothe, 1968; Mohri and Suzuki, 1999; Blavette et al., 1999; Lebyodkin et al., 2000). Most studies to date were focused on the elastic interactions between dislocations and solutes. At low temperatures, diffusion of solutes is negligible, and the solutes act as point obstacles to moving dislocations. Statistical methods (Friedel, 1963; Labusch, 1970) and computer simulations (Sakamoto, 1986; Mohri and Suzuki, 1999) were employed for estimating the dependence of the critical resolved shear stress (CRSS) on solute concentration. At moderate or elevated temperatures where solute diffusion is significant, the elastic interactions between solutes and dislocations lead to solute segregation and depletion around dislocations, leading to the formation of so-called 'Cottrell atmosphere' (Cottrell, 1948). Such a solute atmosphere produces a drag force to a moving dislocation. For a two-dimensional problem with a single dislocation and diffusive solutes, simplified theoretical analysis and numerical calculation of the drag force of the solute cloud on a moving dislocation were presented by Cottrell (1953) and Hirth and Lothe (1968). Asymptotic solute distribution and its dependence on dislocation velocity were analyzed by Hirth and Lothe (1968) and Yoshinaga and Morozumi (1971). Wang et al. (2000) recently developed a kinetic Monte Carlo model for studying the interaction between a single moving edge dislocation and diffusing solute atoms in two dimensions. The solute segregation profile around the moving dislocation, and the relation between the islocation velocity and applied stress were simulated.

Within the continuum mechanics framework, there has been tremendous amount of effort devoted to dislocation dynamics. A number of models (based on the concept of low energy dislocation structures (Bassim et al., 1986), reaction-diffusion approach (Walgraef and Aifantis, 1985a,b; Kubin et al., 1992; Groma and Pawley, 1993), the concept of dislocation sweeping mechanism (Franek et al., 1991; Kratochvil et al., 1997), and stochastic dislocation dynamic description (Hahner, 1996; Bako and Groma, 1990) have been proposed for simulating the formation of dislocation cell structures. A common feature of these models is that the behavior of a dislocation system is described in analogy to other physical problems such as spinodal decomposition, oscillating chemical reactions, etc, at a continuum level. The properties of individual dislocations are taken into account indirectly. Plastic anisotropy, localization and strain rate hardening associated with the formation of dislocation cell structures and evolving microstructures are studied by strain gradient deformation theory (Shizawa and Zbib, 1999; Langlois and Berveille, 2003) and strain hardening model (Barlatb et al., 2002). For discrete dislocation dynamics in 2D and 3D, computer simulations have also been performed by Zbib and Daiz de la Rubia (2002), Hiratani et al. (2003), Groma and Bako (2001), Devincre et al. (2001), Van der Giessen and Needleman (1995), Fivel et al. (1996), Fivel and Canova (1999) and Politano and Salaza (2001). Due to the long range nature of elastic interactions between dislocations, the direct numerical integration of the equation of motion for dislocations is very time-consuming, and thus the size of smulation cell and the number of dislocations are limited.

Recently, Hu and Chen (2001, 2002) proposed a phase-field model by coupling the Cahn–Hilliard diffusion equation (Larcheand, 1982) with the elastic fields produced from solute atoms as well as from structural defects such as precipitates, dislocations, grain boundaries and cracks. In this model, the structural defects are viewed as lattice distortions, and described by 'eigenstrains'. For example, dislocation loops are viewed as coherent misfitting platelet inclusions. Such a description allows us to obtain the elastic fields of defects with arbitrary spatial distribution using the Fourier Transform method (Mura, 1982; Khachaturyan, 1983). This is different from the work based on analytical elastic solution of a dislocation (Leonard and Desai, 1998). A recent significant advance in phase-field modelling of dislocation dynamics was made by Khachaturyan and his associates (Wang et al., 2001a,b). In their phase-field model, the dislocation loops are labeled by a set of order parameter field variables. The temporal evolution of the order parameter fields, i.e., dislocation motion, is described by the phenomenological Time-Dependent Ginzburg–Landau (TDGL) equation (Gunton et al., 1983). Their results show that the model not only can take into account the long-range elastic interaction among dislocations, but also the short range interactions, such as multiplication and annihilation of dislocations.

The main purpose of this paper is to incorporate the solute diffusion into the phase-field model of dislocation dynamics combining the static and dynamic models (Hu and Chen, 2001; Wang et al., 2001a,b). Two sets of field variables, the solute compositional field and order parameter fields describing the dislocation distribution, are employed. The temporal evolution of field variables, thus dislocation motion and solute segregation near the moving dislocation, are obtained by solving the Cahn–Hilliard equation and the TDGL equation, respectively. This model can be used to simulate the dynamic drag effect of solute cloud near moving dislocations, the nucleation of second phase precipitates near dislocations, growth and coherent–incoherent transition, and also the hardening arising from lattice mismatch, elastic modulus difference and long-range order.

The present paper is organized as follows. We start with the phase-field description of an arbitrary dislocation system and the kinetic equations. Next, to validate the model, the stress fields of a dislocation from analytical and numerical methods are compared, and the operation of Frank–Read source in a solid solution is modeled. Finally, the static and dynamic drag effects of Cottrell atmospheres are investigated.

2. Phase field description of a binary system with dislocations

We consider a binary solid solution with a compositional inhomogeneity and a distribution of dislocations. The compositional field $X(\boldsymbol{r}, t)$, representing the mole fraction X at position $\boldsymbol{r}$ at time t, is used to describe the solute distribution. If we assume that the variation of stress-free lattice parameter, a, with composition obeys Vegard's law, then the local stress-free strain caused by compositional inhomogeneity is given by

$$\epsilon^0_{ij}(\mathbf{r}, t) = \epsilon^0 \delta X(\mathbf{r}, t)\delta_{ij}, \tag{1}$$

where $\epsilon^0 = \frac{1}{a}\frac{\mathrm{d}a}{\mathrm{d}X}$ is the composition expansion coefficient of the lattice parameter, $\delta X(\mathbf{r}, t) = X(\mathbf{r}, t) - X_0$ with X_0 being the overall composition of the solid solution, and δ_{ij} is the Kronecker-Delta function.

We recently showed that any structural defects such as dislocations, grain boundaries and slip bands can be introduced into a phase-field model using their corresponding spatially dependent eigenstrains (Mura, 1982; Hu and Chen, 2001). For the case of dislocations, the stress field of a dislocation loop on slip plane p with a Burgers vector $\mathbf{b}$, is described by the stress-free strain (Landau and Lifshitz, 1986; Wang, 2001):

$$\epsilon_{ij}(\mathbf{r}) = \frac{1}{2d_0}(b(i)n(j) + b(j)n(i))\delta(\mathbf{r} - \mathbf{r}_0). \tag{2}$$

where $\mathbf{n}$ is the unit vector normal to the slip plane, d_0 is the interplanar distance of the slip planes, $\delta(\mathbf{r}-\mathbf{r}_0)$ is the Dirac delta function and $\mathbf{r}_0$ is a point inside the dislocation loop on the slip plane. As a matter of fact, $\mathbf{u}_0 = \mathbf{b}\delta(\mathbf{r}-\mathbf{r}_0)$ is the discontinuous displacement field of the atoms above the slip plane relative to those below it.

To describe the temporal evolution of a dislocation system within the context of a phase-field model, Wang et al. (2001a,b) introduced an evolving order-parameter field, $\eta(\mathbf{r}, t)$, which represents the magnitude of the discontinuous relative displacements in units of the Burgers vector $\mathbf{b}$, i.e., $\mathbf{u}_0 = \mathbf{b}\eta(\mathbf{r}, t)$. The stress free strain of a dislocation system is then rewritten as

$$\epsilon^{\mathrm{dis}}_{ij}(\mathbf{r}, t) = \frac{1}{2d_0}(b(i)n(j) + b(j)n(i))\eta(\mathbf{r}, t). \tag{3}$$

For perfect dislocations, $\eta(\mathbf{r}, t)$ should satisfy certain conditions: (i) they should assume non-zero values only inside the dislocation loop; and (ii) these non-zero values should be integers. However, with the definition of eigenstrain given by Eq. (3), it is impossible to satisfy these conditions during dislocation motion under an applied stress. Therefore, one of the main purposes of this paper is to propose a new model to describe the dislocation eigenstrain distribution. We propose to use $f(\eta(\mathbf{r}, t))$ to replace the $\eta(\mathbf{r}, t)$ in expression (3). A particular choice for this function is

$$f(\eta(\mathbf{r}, t)) = \eta(\mathbf{r}, t) - \frac{1}{2\pi}\sin(2\pi\eta(\mathbf{r}, t)). \tag{4}$$

This function $f(\eta(\mathbf{r}; t))$ has the following two properties: (i) It is exactly equal to $\eta(\mathbf{r}, t)$ when $\eta(\mathbf{r}, \mathrm{t})$ is an integer; and (ii) Its derivatives at integer values of $\eta_{\alpha\beta}(\mathbf{r}, t)$ are zero.

Following Wang et al. (2001a,b), the dislocations in a single crystal with N slip systems can be described by N $\left(N = \sum_{\alpha=1}^{p} m_\alpha\right)$ dislocation field variables $\eta_{\alpha\beta}(\mathbf{r}, t)(\alpha = 1, 2, \ldots p; \beta = 1, 2, \ldots, m_\alpha)$, where p denotes the number of elementary slip planes and m_α denotes the number of elementary Burgers vectors

on the slip plane α. For instance, in a FCC single crystal, there are four slip planes: (111), $\left(\bar{1}11\right)$, $\left(1\bar{1}1\right)$, $\left(11\bar{1}\right)$, and three slip directions on each slip plane, and hence it requires 12 dislocation field variables [$p=4$, and $m_\alpha=3$ ($\alpha=1, 2, 3, 4$)]. In a BCC crystal 48 dislocation field variables are needed. Thus, for a given dislocation distribution $\eta_{\alpha\beta}(\mathbf{r}, t)$, the stress-free strain tensor using function (4) can be written as

$$\epsilon_{ij}^{\mathrm{dis}}(\mathbf{r}, t)=\sum_{\alpha,\beta}\frac{b_{\alpha\beta}(i)n_\alpha(j)+b_{\alpha\beta}(j)n_\alpha(i)}{2d_0}f\big(\eta_{\alpha\beta}(\mathbf{r}, t)\big)=\sum_{\alpha,cdb}\epsilon_{ij}^{\mathrm{dis}}(\alpha, \beta)f\big(\eta_{\alpha\beta}(\mathbf{r}, t)\big). \quad (5)$$

In this paper, we introduce 13 field variables to describe the composition $X(\mathbf{r}, t)$ and dislocation distribution $\eta_{\alpha\beta}(\mathbf{r}, t)$ in a model FCC system. The total stress free strain associated with compositional inhomogeneity and an arbitrary distribution of dislocations is then given by

$$\epsilon_{ij}(\mathbf{r}, t)=\epsilon_{ij}^{0}(\mathbf{r}, t)+\epsilon_{ij}^{\mathrm{dis}}(\mathbf{r}, t) \quad (6)$$

3. Thermodynamics of a binary system with dislocations

The temporal evolution of the composition profile and the dislocation distribution is driven by the reduction in the total free energy that include (i) the chemical free energy E^{chem} which consists of both the local bulk free energy of a binary solution and the composition gradient energy; (ii) elastic energy E^{elast} associated with solutes, defects and applied stresses; (iii) a local free energy function with an infinite number of degenerate minima with respect to the order parameters describing a dislocation system, the so-called 'crystalline' energy E^{cryst} (Wang et al., 2001a,b); and (iv) order parameter gradient energy related to the dislocation core energy, E^{grad}.

3.1. The chemical free energy

For a binary system with a spatial composition distribution $X(\mathbf{r})$, the chemical free energy can be described as the sum of two contributions, i.e., the local bulk free energy and the gradient energy. It reads

$$E^{\mathrm{chem}}=\int_v\left[(f_0(X)+\kappa(\nabla X)^2\right]\mathrm{d}v, \quad (7)$$

where the first term $f_0(X)$ is the bulk free energy density of a binary solution; the second term is the gradient energy density, and κ is the gradient energy coefficient. As a model system, we assume a regular solution model,

$$f_0(X)=RT\left[\varphi X(1-X)+X\ln(X)+(1-X)\ln(1-X)\right] \quad (8)$$

where R is the ideal gas constant, T is the absolute temperature, and φ is a material constant. For an ideal solution, φ is equal to zero.

3.2. Elastic energy of the system

Using the concept of stress-free strain/eigenstrain, the calculation of the internal stress field produced by the lattice mismatch due to solutes and dislocations is reduced to finding the elastic solution due to the associated stress-free strains described by Eq. (6) (see Khachaturyan, 1983; Hu and Chen, 2001; Wang et al., 2001a,b for the details). Therefore, once compositional and dislocation distributions in an elastically homogeneous and anisotropic system are known, the total strain energy can be calculated by

$$E^{\text{elast}} = \int_v \frac{1}{2}\lambda_{ijkl}\epsilon_{ij}^{\text{el}}\epsilon_{kl}^{\text{el}}\mathrm{d}v, \tag{9}$$

where

$$\epsilon_{ij}^{\text{el}} = \left[\bar{\epsilon}_{ij} + \delta\epsilon_{ij}(\mathbf{r}) - \epsilon_{ij}^{0}(\mathbf{r}, t) - \sum_{\alpha,\beta}\epsilon_{ij}^{\text{dis}}(\alpha, \beta)f\big(\eta_{\alpha\beta}(\mathbf{r}, t)\big) - \epsilon_{ij}^{\text{def}_0}(\mathbf{r})\right], \tag{10}$$

λ_{ijkl} is the elastic constant tensor, $\bar{\epsilon}_{ij}$ the homogeneous or uniform macroscopic strain characterizing the macroscopic shape and volume change, $\delta\epsilon_{ij}(\mathbf{r})$ heterogeneous strain, and $\epsilon_{kl}^{\text{def}_0}(\mathbf{r})$ the stress-free strain associated with other defects such as precipitates.

3.3. The local free energy density associated with dislocations

Dislocations are lines separating regions which have undergone different degrees of slipping on a given slip plane. For perfect dislocations, these different regions are represented by different integer values of order parameters in the phase-field model, and the difference between the order parameter values of neighboring regions is the total number of dislocations located along the line between them. Therefore, to describe a multiple dislocation system, a local free energy function with an infinite number of degenerate minima is required. One of the free energy functions which satisfy this condition is proposed by Wang et al. (2001a,b) for a crystal with N dislocation slip systems in three dimensions,

$$E^{\text{cryst}} = \int_v \left[\sum_{\alpha=1}^{p}\sum_{\beta=1}^{m_\alpha} A(\alpha, \beta)\sin^2\big(\pi\eta_{\alpha\beta}(\mathbf{r})\big)\right]\mathrm{d}v. \tag{11}$$

Khachaturyan called this 'crystalline energy' simulating the Peierls potential that a dislocation experiences during gliding under an applied stress. However, it should be pointed out that this potential function does not provide a critical stress for the dislocation motion described by the continuum TDGL equation, i.e., the Peierls stress is zero for an isolated dislocation in the perfect crystal in the continuum description.

3.4. Gradient energy associated with dislocation core

In the phase-field model of multi-phases, the energy associated with the composition gradient provides the interfacial energy between different phases. Similarly, the gradient energy in the order parameter fields in the dislocation model describes the dislocation core energy. However, the dislocation core energy is only proportional to the length of a dislocation for perfect dislocations. Wang et al. (2001a,b) proposed the following general form for the gradient term,

$$E^{\text{grad}} = \frac{\gamma}{2}\int_v \Phi(\mathbf{r})\mathrm{d}v \tag{12}$$

where γ is positive constant and the function $\Phi(\mathbf{r})$ is expressed as:

$$\Phi(\mathbf{r}) = \sum_{\alpha_1=1}^{p}\sum_{\alpha_2=1}^{p}\left[\beta(\alpha_1,\alpha_2)_{ijkl}\frac{\partial b(\alpha_1,\boldsymbol{r})_i}{\partial r_j}\frac{\partial b(\alpha_2,\boldsymbol{r})_k}{\partial r_l}\right] \tag{13}$$

$\mathbf{b}(\alpha\ \mathbf{r})$ is the total Burgers vector of dislocations on slip plane α at $\mathbf{r}$.

$$\mathbf{b}(\alpha,\mathbf{r}) = \sum_{\beta=1}^{m_\alpha}\mathbf{b}_{\alpha\beta}\eta_{\alpha\beta}(\mathbf{r}). \tag{14}$$

For dislocation systems $\frac{a_0}{2}\{111\}\langle 110\rangle$ in a FCC crystal, a specific form of the function $\Phi(\mathbf{r})$ is constructed in (Wang et al., 2001a,b).

4. Phase-field kinetic equations

There are two types of evolving objects: solute atoms and dislocations. For the evolution of the solution concentration profile, it is natural to employ the Cahn–Hilliard nonlinear diffusion equation,

$$\frac{\partial X(\mathbf{r},t)}{\partial t} = M\nabla^2\frac{\delta E}{\delta X(\mathbf{r},t)} + \xi(\mathbf{r},t), \tag{15}$$

where X is the composition, E is the total free energy of the system, and M is a kinetic coefficient related to the chemical diffusion mobility. $\xi(\mathbf{r},t)$ is the noise term. Substituting the total energy into the Cahn–Hilliard Eq. (15) and taking the first variational derivatives with respect to the composition function $X(\mathbf{r},t)$, we find that the composition field kinetic equation is

$$\begin{aligned}\frac{\partial X(\mathbf{r},t)}{\partial t} =& M\nabla^2\Big[-\lambda_{ijkl}\epsilon^0\delta_{ij}\big(\epsilon_{ij}+\delta\epsilon_{ij}(\mathbf{r},t)\big)+\lambda_{ijkl}\big(\epsilon^0\big)^2\delta_{ij}\delta_{kl}X(\mathbf{r},t)\\ &+\lambda_{ijkl}\epsilon^0\delta_{ij}\Big[\sum_{\alpha\beta}\epsilon^{\text{dis}}_{kl}(\alpha,\beta)f\big(\eta_{\alpha\beta}(\mathbf{r},t)\big)+\epsilon^{\text{def}_0}_{kl}(\mathbf{r})\Big]\\ &+\frac{\partial f_0(X)}{\partial X}-\kappa\nabla^2X(\mathbf{r},t)\Big]+\xi(\mathbf{r},t).\end{aligned} \tag{16}$$

The order parameter fields describing the dislocation distribution are non-conserved, and their temporal evolution can be assumed to follow the TDGL equations:

$$\frac{\partial \eta_{\alpha\beta}(\mathbf{r}, t)}{\partial t} = -L\frac{\delta E}{\delta \eta_{\alpha\beta}(\mathbf{r}, t)} + \delta(\alpha, \beta, \mathbf{r}, t), \tag{17}$$

where L is the kinetic coefficient characterizing the dislocation mobility, and $\chi(\alpha, \beta, \mathbf{r}, t)$ is the Langevin Gaussian noise term simulating the thermal fluctuations. Eq. (17) can be rewritten as

$$\begin{aligned}\frac{\partial \eta_{\alpha\beta}(\mathbf{r}, t)}{\partial t} = L\Bigg\{ & \lambda_{ijkl}\epsilon_{kl}^{\mathrm{dis}}(\alpha, \beta)\frac{\partial f\big(\eta_{\alpha\beta}(\mathbf{r}, t)\big)}{\partial \eta_{\alpha\beta}(\mathbf{r}, t)}\Bigg[\epsilon_{ij} + \delta\epsilon_{ij}(\mathbf{r}, t) - \epsilon^0\delta_{ij}X(\mathbf{r}, t) \\ & - \sum_{\alpha,\beta}\epsilon_{ij}^{\mathrm{dis}}(\alpha, \beta)f\big(\eta_{\alpha\beta}(\mathbf{r}, t)\big) - \epsilon_{ij}^{\mathrm{def}_0}(\mathbf{r})\Bigg] - A\pi\sin\big(2\pi\eta_{\alpha\beta}(\mathbf{r}, t)\big) \\ & - \frac{\gamma}{2}\frac{\partial \Phi(\mathbf{r}, t)}{\partial \xi\eta_{\alpha\beta}(\mathbf{r}, t)}\Bigg\} + \delta(\alpha, \beta, \mathbf{r}, t)\end{aligned} \tag{18}$$

To facilitate the computation, we introduce the following dimensionless parameters,

$$\begin{aligned} & r^* = \frac{r}{d_0}, d^* = \frac{dx}{d_0}, \varepsilon_0 = \frac{a_0}{d_0} \\ & \lambda_{ijkl}^* = \frac{\lambda_{ijkl}}{G}, \epsilon_{ij}^* = \frac{\epsilon_{ij}}{\varepsilon_0}, \sigma_{ij}^* = \frac{\sigma_{ij}}{G\varepsilon_0} \\ & A^* = \frac{A}{G\varepsilon_0^2}, \gamma^* = \frac{\gamma}{2Gd_0^2\varepsilon_0^2}, t^* = LG\varepsilon_0^2 t \\ & M^* = \frac{M}{Ld_0^2}, \kappa^* = \frac{\kappa}{Gd_0^2\varepsilon_0^2} \\ & f_0^*(X) = \frac{f_0(X)}{G\varepsilon_0^2}, E^{\mathrm{elas}^*} = \frac{E^{\mathrm{elas}}}{G\varepsilon_0^2}, \chi^* = \frac{RT}{G\varepsilon_0^2}\end{aligned} \tag{19}$$

where dx is the grid size of the computational mesh. With the dimensionless parameters, the kinetic equations can be written as:

$$\begin{aligned}\frac{\partial X(\mathbf{r}^*, t^*)}{\partial t^*} = & M^*\nabla^2\Bigg[- \lambda_{ijkl}^*\epsilon^{0*}\delta_{ij}\Big(\epsilon_{kl}^* + \delta\epsilon_{ij}^*(\mathbf{r}^*, t^*)\Big) + \lambda_{ijkl}^*\big(\epsilon^{0*}\big)^2\delta_{ij}\delta_{kl}X \\ & (\mathbf{r}^*, t^*) + \lambda_{ijkl}^*\epsilon^0{*}\delta_{ij}\Bigg[\sum_{\alpha\beta}\epsilon_{kl}^{\mathrm{dis}*}(\alpha, \beta)f\big(\eta_{\alpha\beta}(\mathbf{r}^*, t^*)\big) + \epsilon_{kl}^{\mathrm{def}_0*}(\mathbf{r}^*)\Bigg] \\ & + \frac{\partial f_0^*(X)}{\partial X} - \kappa^*\nabla^2 X(\mathbf{r}^*, t^*)\Bigg] + \xi^*(\mathbf{r}^*, t^*)\end{aligned} \tag{20}$$

$$\frac{\partial \eta_{\alpha\beta}(\mathbf{r}^*, t^*)}{\partial t^*} = \lambda^*_{ijkl}\epsilon^{\mathrm{dis}*}_{jk}(\alpha, \beta)\frac{\partial f\left(\eta_{\alpha\beta}(\mathbf{r}^*, t^*)\right)}{\partial \eta_{\alpha\beta}(\mathbf{r}^*, t^*)}\left[\overline{\epsilon}_{ij} + \delta\epsilon_{ij}(\mathbf{r}, t) - \epsilon^{0*}\delta_{ij}X(\mathbf{r}^*, t^*)\right.$$
$$\left. - \sum_{\alpha,\beta}\epsilon^{\mathrm{dis}*}_{ij}(\alpha, \beta)f\left(\eta_{\alpha\beta}(\mathbf{r}^*, t^*)\right) - \epsilon^{\mathrm{def}_0*}_{ij}(\mathbf{r}^*)\right]$$
$$- A^*\pi\sin\left(2\pi\eta_{\alpha\beta}(\mathbf{r}^*, t^*)\right) - \gamma^*\frac{\partial\Phi(\mathbf{r}^*, t^*)}{\partial\xi\eta_{\alpha\beta}(\mathbf{r}^*, t^*)} + \delta^*(\alpha, \beta, \mathbf{r}^*, t^*) \qquad (21)$$

The elastic equilibrium equation and the kinetic equations are solved numerically. The semi-implicit spectral method (Chen and Shen, 1998) is employed, which implies the use of periodic boundary conditions along x-, y- and z-directions. In all the simulations, we fix the following parameters: $C_{11}=3.0$, $C_{12}=1.0$, $C_{44}=1.0$, $A^*=0.05$ $\gamma^*=0.25$, $\kappa^*=0.05$, $\epsilon^0=0.075$, $X^*=0.09$, $\epsilon_0=0.25$, $dt^*=0.02$, $d^*=1.0$, $d_0=4a_0$ where a_0 is the lattice parameter. We systematically vary the dimensionless parameters M^*, φ, X_0 and $\overline{\epsilon}^*_{ij}$ to study their effect on dislocation–solute interactions under applied stresses. In addition, we do not consider the effect of immobile defects, i.e., $\epsilon^{\mathrm{def}_0}_{kl}(\mathbf{r}^*)=0$ in the present paper. The influence of elastic anisotropy, elastic inhomogeneity and immobile defects will be presented in future publications.

5. Result and discussion

5.1. Stress fields of dislocations

Before the solute–dislocation interactions are studied, the stress field of a dislocation described by the dislocation eigenstrain (5) is examined. Since an analytical elastic solution exists for a single edge dislocation in two dimensions, we consider a two-dimensional model system shown in Fig. 1. We assume that the composition of

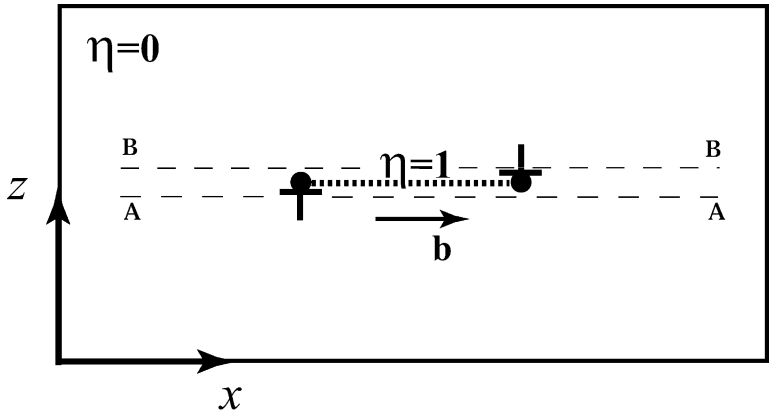

Fig. 1. Schematic illustration of a dislocation loop located at the center of a 2D computational cell.

solutes is zero or uniform and does not evolve with time. A dislocation loop with $R = 120dx$ is introduced into the center of the simulation cell 512×512 by assigning the initial value $\eta = 1$ on the grid points inside the dislocation loop on the slip plane and $\eta = 0$ outside the loop. The Burgers vector of the dislocation loop is $\mathbf{b} = (100)$ along the x-direction, and its slip plane is the $\mathbf{n} = (001)$ plane. The equilibrium solution of kinetic Eq. (21) in the absence of applied stresses automatically provides the stress field of the dislocation. In Fig. 2 we present the normal and shear stress distributions of the edge dislocation in the right side of simulation cell along A–A line just below the slip plane shown in Fig. 1. The corresponding analytical solution is also plotted for comparison. The results demonstrate that the stress fields obtained with the new expression of dislocation eigenstrains are in good agreement with the analytical elastic solution except for two or three points where the stresses of analytical solutions are singular. In addition, we can find that numerical stresses are continuous at the dislocation line. This means that the singularity of the stress field at the dislocation line is removed. It is a natural result if we notice that the discontinuous displacement at a dislocation line in classical elastic theory is replaced by a continuous displacement in the phase field model. Therefore, phase field models of dislocations provide similar elastic stress fields as nonlocal elastic theory (Walgraef and Aitantis, 1985a,b). The elimination of singularity not only brings the dislocation stress field much closer to the real situation but also benefits the stability of numerical calculation.

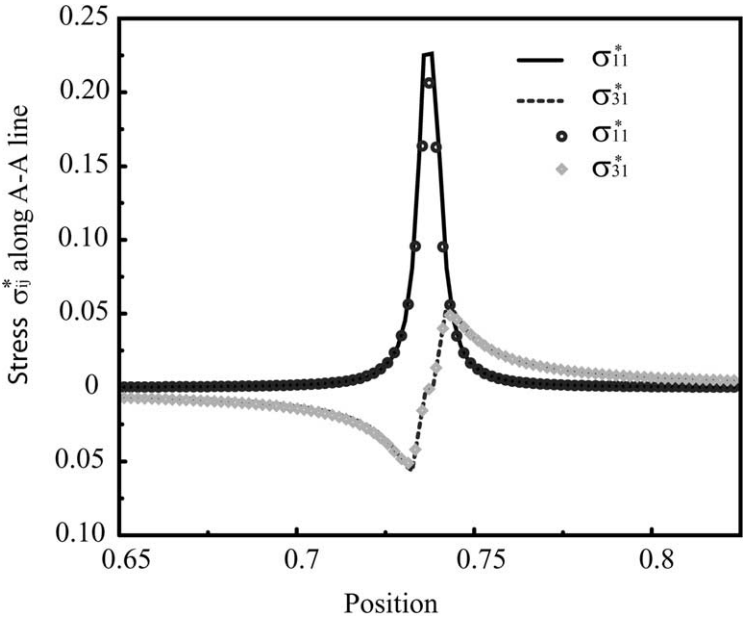

Fig. 2. Comparison of dislocation stress distributions calculated from numerical and analytical solutions along A–A line shown in Fig. 1, the solid lines for analytical solution and the symbol lines for numerical solutions.

Although linear expression (3) (Wang et al., 2001a,b) can also provide correct stress fields of static dislocations, it results in the dependence of the magnitude of the dislocation Burgers vector on applied stresses. Hence, it might lead to incorrect stress fields of moving dislocations. To examine the effect of two dislocation eigenstrain expressions on the stress field of moving dislocations, the kinetic Eq. (21) is solved under different applied shear stresses $\bar{\sigma}^*_{31}$. Fig. 3 shows the temporal order parameter profiles at $t^* = 400dt^*$, $800dt^*$, $1200dt^*$ and $1600dt^*$ with a loading history $\bar{\sigma}^*_{31} = 0.0$, 0.015, 0.02 and 0.025 for every 400 time steps. The related shear stress

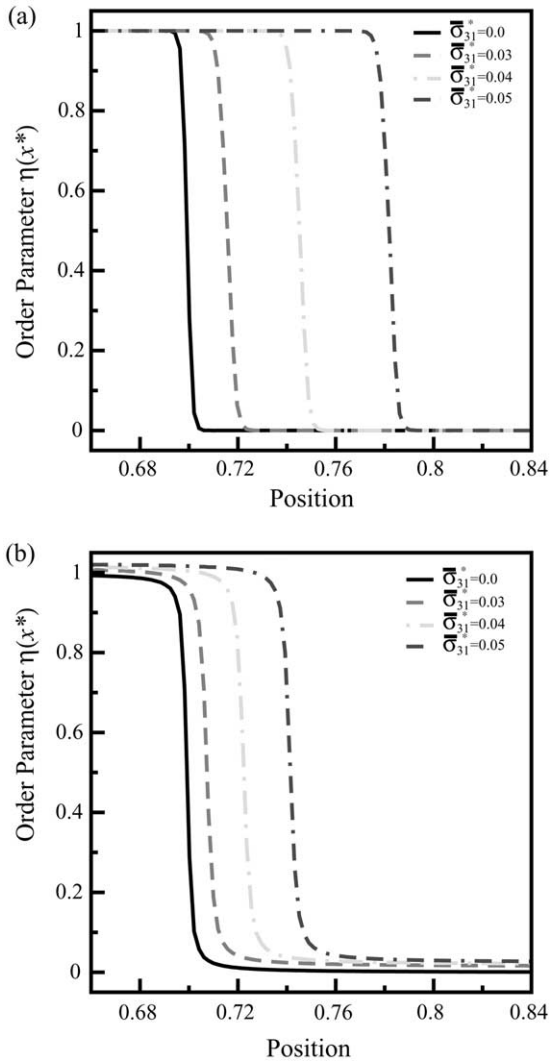

Fig. 3. Order parameter profiles under different applied stresses $\bar{\sigma}_{31}$, (a) with the non-linear expression of dislocation eigenstrain, (b) with the linear expression of dislocation eigenstrain.

distributions on the slip plane are plotted in Fig. 4. It is observed in Fig. 3(b) that the order parameter values inside and outside the dislocation loop increase with the magnitude of the applied stress for the case that the dislocation eigenstrain expression is a linear function of the order parameter in Eq. (3). This implies that dislocation Burgers vector depends on applied stresses. From Fig. 4(b), we can see that

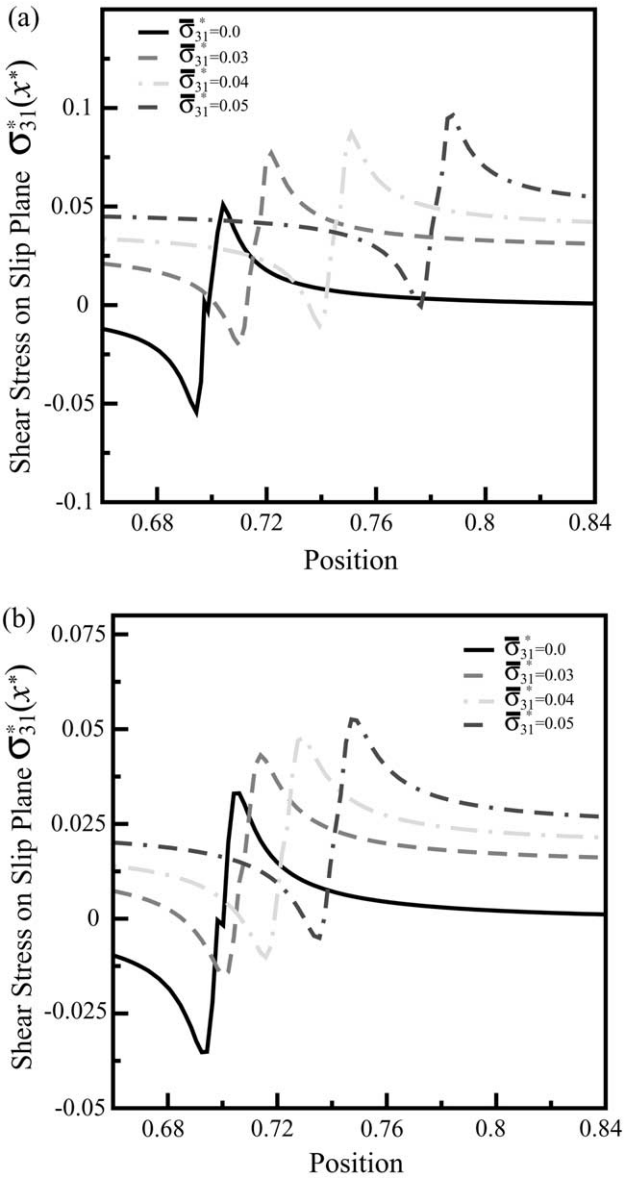

Fig. 4. Shear stress distributions along the slip plane for moving dislocations.

an extra stress field due to the change of Burgers vector greatly reduces the effect of the applied stress. As a result, the extra stress slows down the dislocation velocity. However, the nonlinear eigenstrain expression (5) proposed in the present paper eliminates this dependence. The order parameter profiles in Fig. 3(a) show that the order parameter values away from the dislocation core do not change under applied stresses with the new eigenstrain expression. The applied stresses affect only the order parameter profile in the dislocation core. Therefore, the dislocation stress field away from the dislocation core remains the same during dislocation motion under different applied stresses, which can be seen from Fig. 4(a). These results demonstrate that the new dislocation eigenstrain expression can provide a correct stress field for both static and moving dislocations. It should be pointed out that the internal stress fields produced by other crystal defects such as other dislocations and cracks will also lead to a change in the Burgers vector if the linear eigenstrain expression is employed. Such dependency is eliminated using the new eigenstrain expression.

5.2. Velocities of dislocations and discretization effect

To examine the relationship between the velocity of a dislocation and the applied stress, the motion of dislocations in two dimensions shown in Fig. 1 is simulated under different applied stresses. The velocities (the displacement of the dislocation within a fixed number of time steps) are calculated. Fig. 7(a) shows the velocity of the dislocation as a function of applied stresses and grid sizes for eigenstrain expressions (5). There are three observations. First, the dislocation velocity strongly depends on the grid size (i.e., discretization effect). It increases as the grid size decreases for a given applied stress. However, the velocity is convergent when the gride size d^* is less than 1.0. Second, a linear relationship between the dislocation velocity and the applied stress exists for the convergent cases. Using phase-plane analysis approach (Grindrod, 1991), a relationship between the dislocation velocity V^* and the applied stresses for an edge dislocation in two dimensions is derived

$$V^* = \frac{2\bar{\sigma}^*_{31}\epsilon^{\mathrm{dis}^*}_{31}}{\int_0^1 \eta_0'(x^*)d\eta_0} = S^*\bar{\sigma}^*_{31} \tag{22}$$

where $\eta_0'(x^*)$ is the solution of Eq. (21) in the absence of applied stress. Eq. (21) for an dislocation loop in two dimensions shown in Fig. 1 reads

$$2\gamma^*\eta_0'' - A^*\pi\sin(2\pi\eta_0) + 2\sigma^*_{31}/\epsilon^{\mathrm{dis}}_{31}\frac{\partial f(\eta_0)}{\partial_{\eta_0}} = 0 \tag{23}$$

where σ^*_{31} is the stress component of the dislocation (Hu et al., in preparation). The value $S = 5.3(d_0/t^*)$ calculated with Eq. (22) is in good agreement with the numerical result $S = 5.1(d_0/t^*)$ for the convergent cases. Finally, the fact, that the velocity tends to zero as the applied stress tends to zero, implies that no critical stress exists for moving an isolated dislocation. In other words, Peierls stress is not taken into account in this phase field model although the total energy includes the term 'Peierls

potential'. Any critical stress appearing in the cases with larger gride sizes comes from discretization effect. For a comparison, the same simulations are performed by using eigenstrain expressions (3). Similar discretization effect is observed. From Fig. 7 (b), it can be found that the velocity obtained by using eigenstrain expressions (3) is much smaller than that obtained by using eigenstrain expressions (5) under the same applied stress. This is consistent with the discussion in the last section that part of the work done by the applied stress is spent on increasing the Burgers vector of the dislocation for the case of eigenstrain expressions (3), and hence the corresponding dislocation velocity is reduced.

5.3. *Effect of solutes on dislocation generation through Frank–Read source*

With the new expression of dislocation eigenstrains, we examined whether it is possible to generate dislocations from a Frank–Read source as well as the effect of solute segregation on dislocation generation. A square dislocation loop is placed on the slip plane $(11\bar{1})$ in $128\times128\times128$ simulation cell by assigning $\eta_{11}(\mathbf{r})=1$ on the grid points in the region marked by the gray color and $\eta_{11}(\mathbf{r})=0$ on other grid points as shown in Fig. 5. The Burgers vector of the dislocation loop is $(\bar{1}10)$. The simulation parameters are set to be $X_0=0.1$; $M^*=1.0$ and $\varphi=1.5$. A pure shear stress field ($\bar{\tau}^*=0.06$) along $[\bar{1}10]$ is applied on the (111) plane. Fig. 6(a)–(c) shows snapshots of dislocation generation on the (111) plane by the Frank–Read source

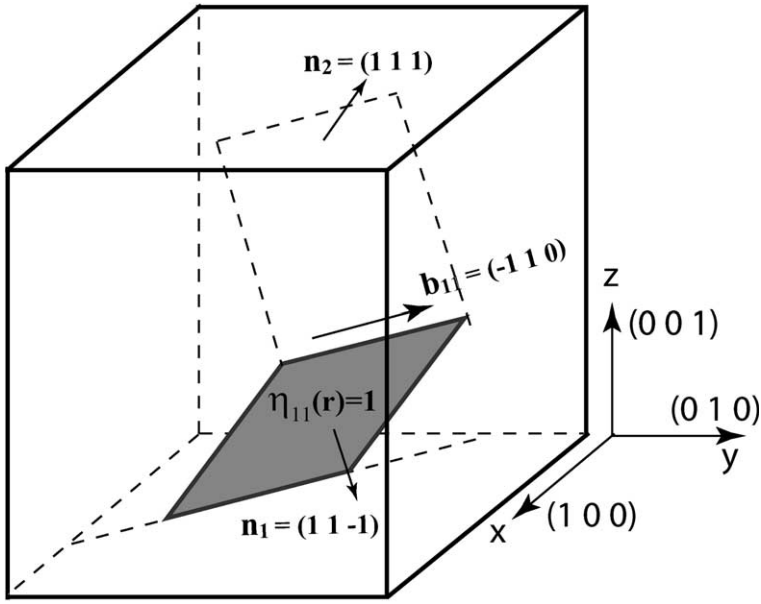

Fig. 5. Schematic illustration of simulation cell of Frank–Read source.

mechanism. The light gray and dark gray surfaces in Fig. 6 (d)–(f) are the iso-surfaces ($X(\mathbf{r})=0.11$) and ($X(\mathbf{r})=0.09$) of composition distributions, respectively. The results show that new dislocation loops with the same Burgers vector nucleate on slip plane (111) near the screw segment of the dislocation loop on slip plane $(11\bar{1})$ under the shear stress on the slip plane (111). With the increase of applied stresses, one part of the new dislocation loop bows out on the slip plane (111), the other part annihilates at the intersection line between (111) and $(11\bar{1})$ slip planes because these two screw dislocation segments have opposite Burgers vectors, and its two ends are pinned by the edge dislocation on the $(11\bar{1})$ plane. The Frank–Read source can continuously emit dislocation loops as shown in Fig. 6(c). Since the lattice mismatch of solutes is assumed to be a uniform expansion $\epsilon^0=0.075$, the interaction between the edge segment and solutes results in solutes segregating on the tensile side of the edge dislocation segment. No segregation and depletion is observed near screw dislocation segments since there is no volume change near a pure screw dislocation. Because the dislocation segment involved in Frank–Read source operation is mainly the screw component, solute segregation has minimal effect on the Frank–Read source operation. The main effect of solute segregation is the reduction in the dislocation velocity for the edge segment compared with the case without solutes.

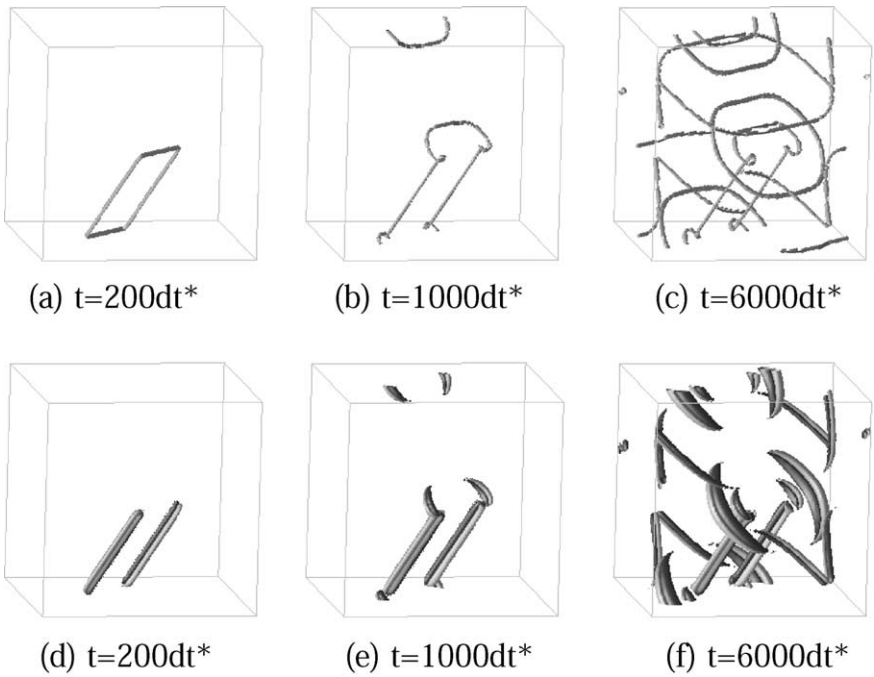

Fig. 6. Snapshot pictures of the dislocation generation on (111) plane by Frank–Read mechanism in solid solution.

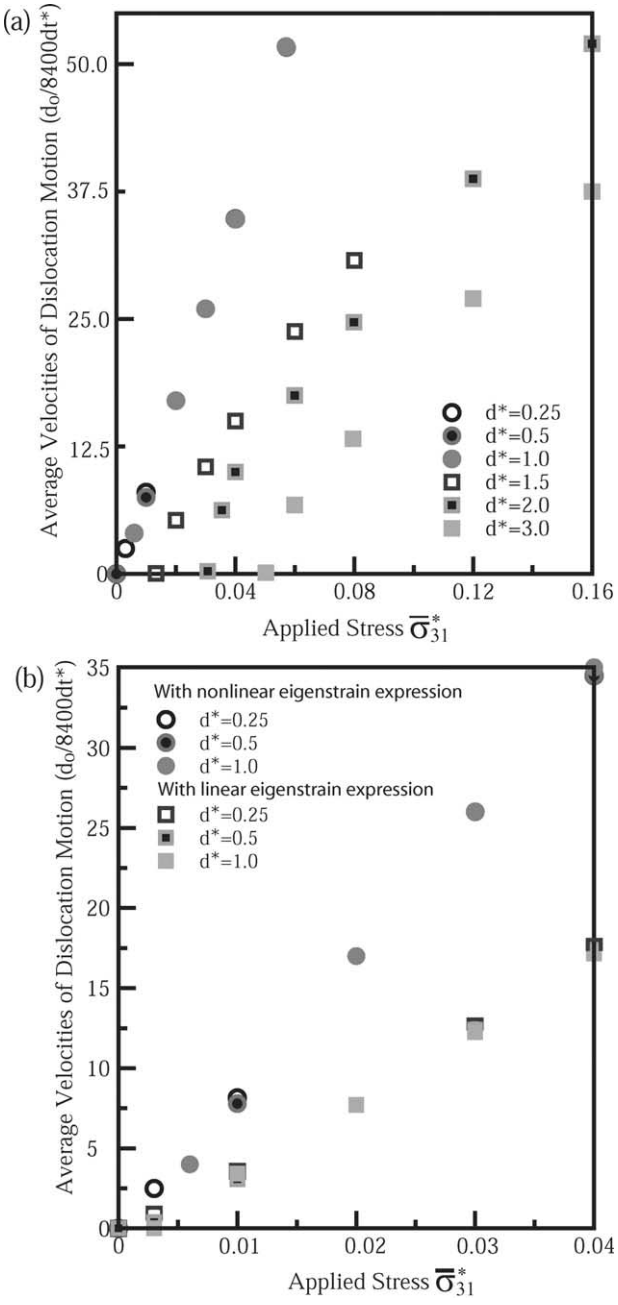

Fig. 7. Average velocities of dislocations vs. applied shear stresses, (a) the effect of different eigenstrain expressions, (b) the effect of discretization.

5.4. Drag of dislocation motion by Cottrell atmosphere

If the sizes of solvent and solute atoms in a binary system are significantly different, the stress field of an edge dislocation leads to a segregation of solutes around the dislocation, i.e., the formation of the so-called Cottrell atmospheres. Solute segregation partially releases the stress field of dislocations and generates resistance to dislocation slip. The interaction between dislocations and solutes strongly depends on solute mobilities and dislocation velocities. If the solute diffusion velocity is much larger than the dislocation velocity, an equilibrium solute atmosphere is established near a moving dislocation. In this case a static drag of dislocation motion by a Cottrell atmosphere occurs. When the velocity of solute diffusion is compatible with the dislocation velocity, Portevin LeChatelier instabilities (dynamic strain aging) might occur, which is related to the dynamic drag of dislocation motion by a Cottrell atmosphere. In another extreme case, there is no Cottrell atmosphere formed if the solute diffusion is much smaller than the dislocation velocity.

5.4.1. Static drag effect of a Cottrell atmosphere

To calculate the static drag effect of a Cottrell atmosphere, we first need to obtain the equilibrium distribution of solute atoms near a dislocation. Since the driving force for solute diffusion is due to the inhomogeneity of elastic and chemical potentials, the equilibrium distribution of solutes depends on the competition between elastic energy and chemical free energy. To examine the effect of φ on solute equilibrium distribution, three solid solutions with $\varphi = 0.0$; 1.5 and 3.0 are considered. Their chemical free energies are plotted in Fig. 8.

A dislocation loop with $R = 120dx$ is placed at the center of a two-dimensional 512×512 simulation cell. We start the simulation with different initial average composition X_0 marked with the vertical dash lines in Fig. 8, and stop the simulation when the solute atoms reach equilibrium. For a solution with average composition $X_0 = 0.05$, the equilibrium solute distributions along A–A and B–B lines shown in Fig. 1 are presented in Fig. 9 for different free energy functions. Fig. 10 shows the equilibrium solute distributions for an ideal solution $\varphi = 0.0$ with different initial average composition $X_0 = 0.05$, 0.25 and 0.50, respectively. The results demonstrate that solute segregation and depletion are usually not symmetric with respect to the dislocation slip plane. For example, in the case of average composition $X_0 = 0.05$, the minimum composition located on the B–B line in solute-depleted region is almost independent of φ. However, the maximum composition located on the A–A line in solute-enriched region increases with φ. The net increase of solute composition at the maximum composition point is much larger than the net decrease at the minimum composition point. From mass balance, this implies that the depleted region is larger than the solute-enriched region. It is also true even for an ideal solution shown in Fig. 10 except for the case with the average solute composition 0.5 at which the chemical free energy is symmetric with respect to composition while the stress field of dislocation is antisymmetric. Therefore, the symmetric solute distribution around a dislocation predicted by the analytical solution (Hirth and Lothe, 1968) is only valid for the case of an ideal solid solution with an average composition 0.5.

To compute the interaction between a dislocation and its solute atmosphere, we freeze the solute distribution while the dislocation is artificially displaced along the slip plane. Since only elastic energy changes during the process of dislocation displacement, the total elastic energy of the system as a function of dislocation displacement is plotted in Fig. 11. The drag force exerted on the dislocation by the

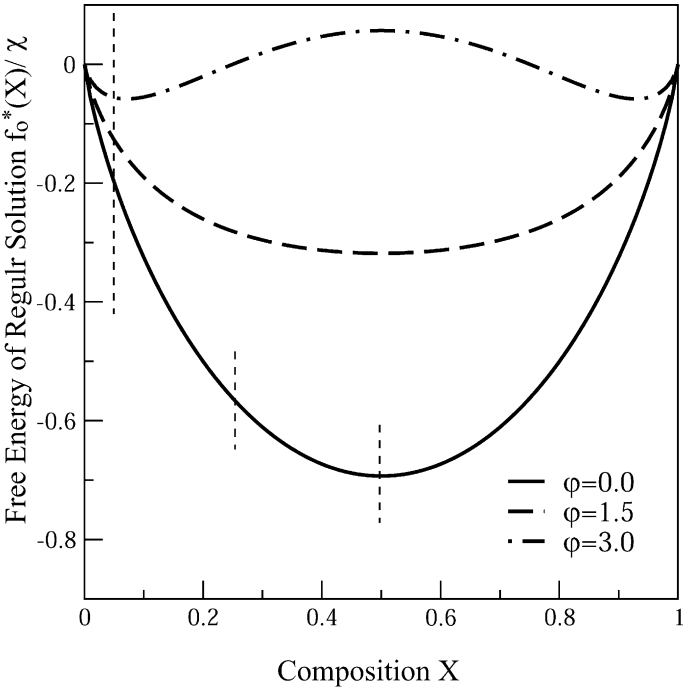

Fig. 8. Chemical free energies of solid solutions.

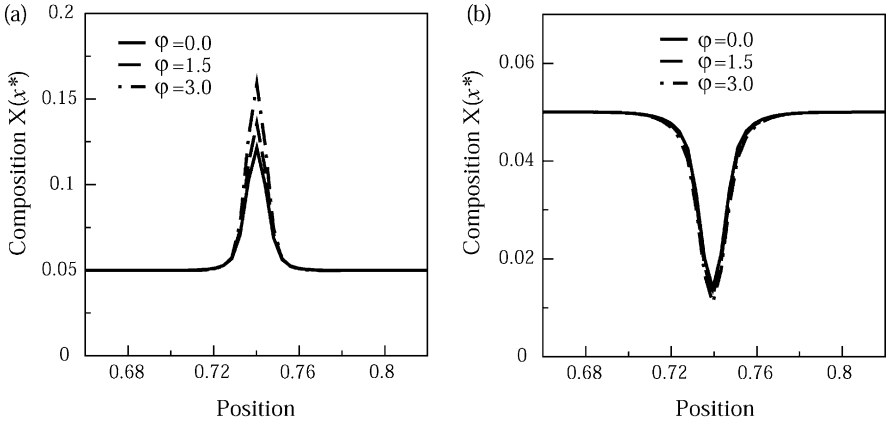

Fig. 9. Equilibrium solute distributions, (a) along *A–A*, (b) along *B–B* line shown in Fig. 1.

solute atmosphere at a given displacement is proportional to the gradient of elastic energy–displacement curve. The maximum drag force occurs at the point where the elastic energy–displacement curve reaches its maximum gradient. When external forces are less than the maximum drag force, the dislocation cannot break away from the solute cloud. From Fig. 11, we can see that the maximum drag force depends on the chemical free energy function and the average solute composition. Increases in both the average composition X_0 and φ enhance the solute segregation as shown in Figs. 8 and 9 and hence increase the drag force of a Cottrell atmosphere to dislocation motion.

5.4.2. Dynamic drag effect of a Cottrell atmosphere

Dynamic drag effect of a Cottrell atmosphere critically depends on the relative velocities of solute diffusion and dislocation motion. In our simulations, we fix the magnitude of the applied stress $\bar{\sigma}^*_{31} = 0.04$ and the lattice mismatch between solute and solvent atoms $\epsilon^0 = 0.075$ while varying the ratio M^* of the solute mobility to the dislocation mobility or the average composition X_0. The simulation cell is chosen to be 512×256 grid points, and the dimensionless parameters are the same as that listed in Section 4. The initial radius of the dislocation loop is $R = 80dx$. Fig. 12 shows the average velocity of a dislocation as a function of M^* and X_0. From the results, we can see that dislocation velocity decreases as the overall composition X_0 increases for a given M^*. The reason is that the higher overall composition results in higher degree of segregation, and thus a larger dragging force. Furthermore, three characteristic velocities of dislocations can be observed from Fig. 12 for any given overall solute composition. One extreme case is that M^* tends to zero. This implies that solute diffusion becomes very slow compared with dislocation velocity. As a result, solute segregation and its dragging force are negligible, and the dislocation velocity reaches the maximum. Another extreme case is that solutes diffuse fast enough to be able to fully catch the moving dislocation. In this case, a steady-state solute atmosphere, which is close to the equilibrium distribution around a static dislocation,

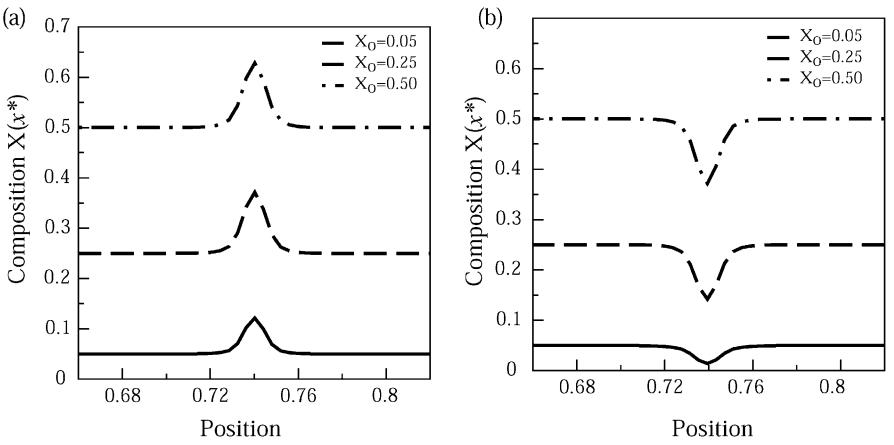

Fig. 10. Equilibrium solute distributions, (a) along *A–A*, (b) along *B–B* line shown in Fig. 1.

forms around the moving dislocation. The average dragging stress becomes constant, and dislocation moves with a constant velocity. It is also seen that a proper ratio M^* of solute diffusion mobility and dislocation mobility causes the dislocation moving with a minimum velocity. From the results it can be found that such a M^* is

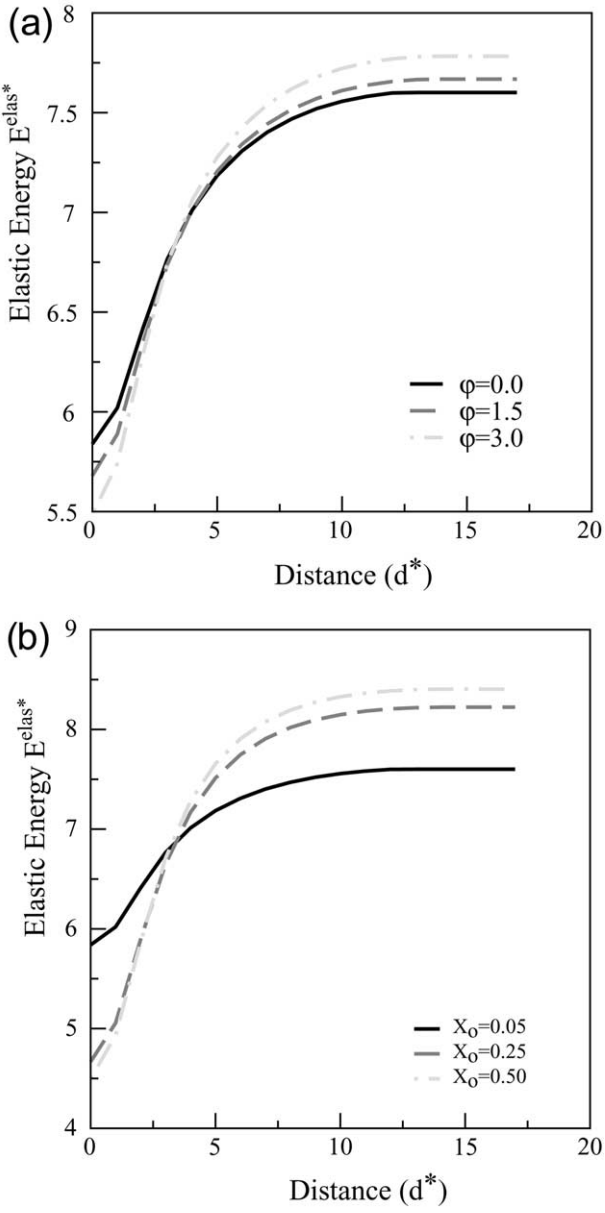

Fig. 11. Corresponding elastic energy E^{elas*}-dislocation–displacement curve, (a) for different φ, (b) for different average compositions.

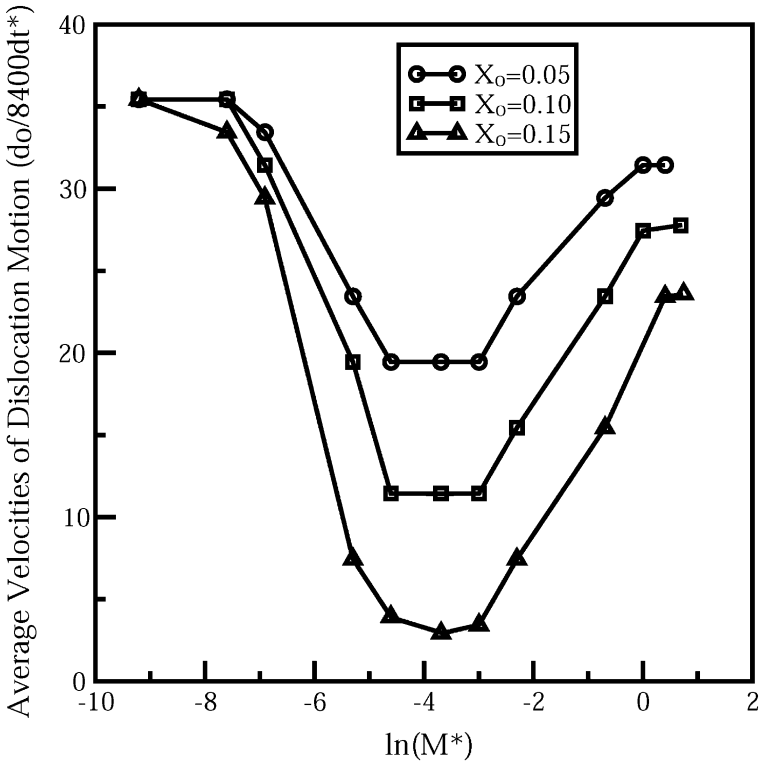

Fig. 12. Average velocity of dislocations is a function of M^* for different average compositions at constant applied stresses $\bar{\sigma}_{31} = 0.04$.

independent of solute overall composition. In this region, solute diffusion is compatible with dislocation velocity. Examination of the solute distribution and dislocation velocity as a function of time shows that the solute distribution and the dislocation velocity change periodically during dislocation motion. In other words, Portevin LeChatelier instabilities occur in this region. A detailed and quantitative study of Portevin LeChatelier instabilities associated with the solute dynamic drag effect will be presented in a future publication.

6. Conclusion

A phase field model is described for modelling the interactions between moving dislocations and diffusive solutes. The results showed that the new expression for dislocation eigenstrain used in the present paper is able to eliminate the dependence of dislocation Burgers vector on applied stresses, and provide correct stress fields for static and dynamic dislocations. Theoretical analysis and numerical simulations demonstrate that the velocity of the dislocation is proportional to the applied stress,

and the phase field model does not take into account the Peierls stress. Although the main simulations in the present paper are conducted in two dimensions with a single dislocation, these simulations confirmed the potential ability of phase field models for investigating dislocation dynamics coupling with other important physical processes such as solute diffusion.

Acknowledgements

We are grateful for the financial support from NSF under the grant No. DMR-01-22638 and from ALCOA. We also thank H. Weiland and J. Murray for helpful discussions. The simulations were performed at the San Diego Supercomputer Center and the Pittsburgh Supercomputing Center. Yuxi Zheng is partially supported by grant NSF DMS-0071858.

References

Bako, B., Groma, I., 1999. Stochastic approach for modeling dislocation pattering. Phys. Rev. B 60, 122.
Barlat, F., Glazov, M.V., Brem, J.C., Lege, D.J., 2002. A simple model for dislocation behavior, strain and strain rate hardening evolution in deforming aluminum alloys. Int. J. Plasticity 18, 919.
Bassim, M.N., Jesser, W.A., Kuhlmann-Wilsdorf, D., Wilsdorf, H.G., 1986. Low-energy dislocation structures. Mater. Sci. Engng. 81, 1.
Blavette, D., Cadel, E., Fraczkiewicz, A., Menand, A., 1999. Three-dimensional atomic-scale imagining of impurity segregation to line defects. Science 286, 2317.
Chen, L.Q., Shen, J., 1998. Applications of semi-implicit fourier-spectral method to phase field equations. Comput. Phys. Commun. 108, 147.
Cottrell, A.H., 1948. Report on strength of solids. In: Proc. Phys. Soc., Lond., 30.
Cottrell, A.H., 1953. Dislocations and Plastic Flow in Crystals. Oxford University Press, London.
Devincre, B., Kubin, L.P., Lemarchand, C., Madec, R., 2001. Mesoscopic simulations of plastic deformation. Mater. Sci. Eng. A 309, 211.
Fivel, M.C., Canova, G.R., 1999. Developing rigious boundary conditions to simulations of discrete dislocation dynamics. Model. Simul. Mater. Sci. Eng. 7, 753.
Fivel, M.C., Gosling, T.J., Canova, G.R., 1996. Implementing image stresses in a 3D dislocation simulation. Model. Simul. Mater. Sci. Eng. 4, 581.
Franek, A., Kalus, R., Kratochvil, J., 1991. Model of early stage of dislocation structure formation in cyclically deformed metal crystals. Phlos. Mag. A 64, 497.
Friedel, J., 1963. Electron Microscopy and Strength of Crystals. Interscience, New York.
Grindrod, P., 1991. Patterns and Waves: The Theory and Applications of Reaction Diffusion Equations. Clarendon Press, Oxford.
Groma, I., Pawley, G.S., 1993. Computer simulation of plastic behaviour of single crystals. Philos. Mag. A 67, 1459.
Groma, I., Bako, B., 2001. Linking different scales: discrete, self-consistent field, and stochastic dislocation dynamics. Mater. Sci. Eng. A309–310, 356.
Gunton, J.P., Miguel, M.S., Sahni, P.S. In: Domb, C., Lebowitz, J.L. (Eds.), Phase Transitions and Critical Phenomena, Vol. 8. Academic Press, New York, p. 267.
Haasen, P., 1964. A model for the nucleation of a spherical coherent precipitate near an edge dislocation. In: Nabarro, F.R.N. (Ed.), Dislocations in Solids 4.
Hahner, P., 1996. A theory of dislocation cell formation based on stochastic dislocation dynamics. Acta Mater. 44, 2345.

Hiratani, M., Zbib, H.M., Khaleel, 2003. Modeling of thermally activated dislocation glide and plastic flow through local obstacles. Int. J. Plasticity 19, 1271.
Hirth, J.P., Lothe, J., 1968. Theory of Dislocation. McGraw-Hill, New York.
Hu, S.Y., Chen, L.Q., 2001. Solute segregation and coherent nucleation and growth near a dislocation—a phase field model integrating defect and phase microstructures. Acta Mater. 49, 463.
Hu, S.Y., Chen, L.Q., 2002. Diffuse-interface modeling of composition evolution in the presence of structural defects. Comput. Mater. Sci. 23, 270.
Hu, S.Y., Zheng, Y.X., Chen, L.Q., Quantitative phase-field modeling of dislocation dynamics (in preparation).
Khachaturyan, A.G., 1983. Theory of Structural Transformations in Solids. John-Wiley and Sons.
Kratochvil, J., Saxlova, M., Devincre, B., Kubin, L.P., 1997. On the sweeping of dipolar loops by gliding dislocations. Mater. Sci. Eng. A234–236, 318.
Kubin, L.P., Canova, G., Condat, M., Devincre, B., Pontikis, V., Brechet, Y., 1992. Dislocation microstructures and plastic flow: a 3D simulation. Solid State Phenomena 23–24, 455.
Labusch, R., 1970. A statistical theory of solid solution hardening. Phys. Stat. Solidi 41, 659.
Landau, L.D., Lifshitz, E.M., 1986. Theory of Elasticity. Pergamon Press, New York.
Langlois, L., Berveiller, M., 2003. Overall softening and anisotropy related with the formation and evolution of dislocation cell structure. Int. J. Plasticity 19, 599.
Larcheand, F.C., Cahn, J.W., 1982. The effect of self-stress on diffusion in solids. Acta Metall. 30, 1835.
Lebyodkin, M., Dunin-Barkowskii, L., Brechet, Y., Estrin, Y., Kubin, L.P., 2000. Spatio-temporal dynamics of the Portevin-Le Chatelier effect: experiment and modelling. Acta Mater. 48, 2529.
Leonard, F., Desai, R., 1998. Spinodal decomposition and dislocation lines in thin films and bulk materials. Phys. Rev. B 58, 8277.
Mohri, T., Suzuki, T., 1999, Solid solution hardening by impurities. In Briant, C.L. (Ed.), Impurities in Engineering Materials, p. 259.
Mura, T., 1982. Micromechanics of Defects in Solids. Kluwer Academic.
Politano, O., Salazar, J.M., 2001. A 3D mesoscopic approach for discrete dislocation dynamics. Mater. Sci. Eng. A309–310, 261.
Sakamoto, M., 1986. Dragging stress exerted on edge dislocation moving with solute atomosphere in highly concentrated solid solutions. J. Appl. Phys. Jpn. 56, 3201.
Shizawa, K., Zbib, H.M., 1999. A thermodynamic theory gradient elastoplasticity with dislocation density tensor. I: fundamentals. Int. J. Plasticity 15, 899.
Van der Giessen, E., Needleman, A., 1995. Discrete dislocation plasticity: a simple planar model. Model Simul. Mater. Sci. Eng. 3, 689.
Walgraef, D., Aifantis, E.C., 1985a. Dislocation pattering in fatigued metals as a result of dynamical instabilities. J. Appl. Phys. 15, 688.
Walgraef, D., Aifantis, E.C., 1985b. On the formation and stability of dislocation patterns—iii: three-dimensional considerations. Int. J. Engng. Sci. 23, 1365.
Wang, Y., Strolovitz, D.J., Rickman, J.M., Lesar, R., 2000. Dislocation motion in the presence of diffusing solutes: a computer simulation study. Acta Mater. 48, 2163.
Wang, Y.U., Jin, Y.M., Cuitino, A.M., Khachaturyan, A.G., 2001a. Phase field microelasticity theory of dislocation dynamics in a polycrystal: model and three-dimensional simulations. Phil. Mag. Lett. 81, 607.
Wang, Y.U., Jin, Y.M., Cuitino, A.M., Khachaturyan, A.G., 2001b. Phase field microelasticity theory and modeling of multiple dislocation dynamics. Appl. Phys. Lett. 16, 2324.
Yoshinaga, H., Morozumi, S., 1971. The solute atmosphere round a moving dislocation and its dragging stress. Philos. Mag. 23, 1367.
Zbib, H.M., Daiz de la Rubia, Tomas, 2002. A multiscale model of plasticity. Int. J. Plasticity 18, 1133.